PHILOSOPHICAL TRANSACTIONS OF THE ROYAL SOCIETY A

rsta.royalsocietypublishing.org

Review

Cite this article: Garcia JV, Zhang F, Ford PC. 2013 Multi-photon excitation in uncaging the small molecule bioregulator nitric oxide. Phil Trans R Soc A 371: 20120129.
http://dx.doi.org/10.1098/rsta.2012.0129

One contribution of 18 to a Discussion Meeting Issue 'Photoactivatable metal complexes: from theory to applications in biotechnology and medicine'.

Subject Areas:
inorganic chemistry

Keywords:
nitric oxide, two-photon excitation, upconversion nanoparticles, photochemistry

Author for correspondence:
Peter C. Ford
e-mail: ford@chem.ucsb.edu

Royal Society Publishing
Informing the science of the future

Multi-photon excitation in uncaging the small molecule bioregulator nitric oxide

John V. Garcia[1], Fan Zhang[2] and Peter C. Ford[1]

[1]Department of Chemistry and Biochemistry, University of California, Santa Barbara, CA 93106, USA
[2]Department of Chemistry, Shanghai Key Laboratory of Molecular Catalysis, and Laboratory of Innovative and Advanced Materials, Fudan University, Shanghai 200433, People's Republic of China

Multi-photon excitation allows one to use tissue transmitting near-infrared (NIR) light to access excited states with energies corresponding to single-photon excitation in the visible or ultraviolet wavelength ranges. Here, we present an overview of the application of both simultaneous and sequential multi-photon excitation in studies directed towards the photochemical delivery ('uncaging') of bioactive small molecules such as nitric oxide (NO) to physiological targets. Particular focus will be directed towards the use of dyes with high two-photon absorption cross sections and lanthanide ion-doped upconverting nanoparticles as sensitizers to facilitate the uncaging of NO using NIR excitation.

1. Introduction

The goal of this article is to offer a somewhat personalized overview of efforts in our laboratory and in others to use multi-photon excitation for the delivery of 'caged' bioactive substances to physiological targets.[1] In general, the use of photo-excitation as the external trigger allows one to define the *location* and *timing* of the release (or 'uncaging') of such species. Furthermore, since the extent of photochemical reaction is a function of the amount of light absorbed by the reactive precursor, this allows one to define also the *dosage* of the release. Reactions may be triggered by single-photon absorption or (in some cases) by multi-photon absorption, and the ensuing discussion will compare these pathways.

[1]'Caged' compounds are bio-inactive in one molecular form but are transformed photochemically (typically by fragmenting) to give a bioactive component. The latter process is often called 'uncaging'.

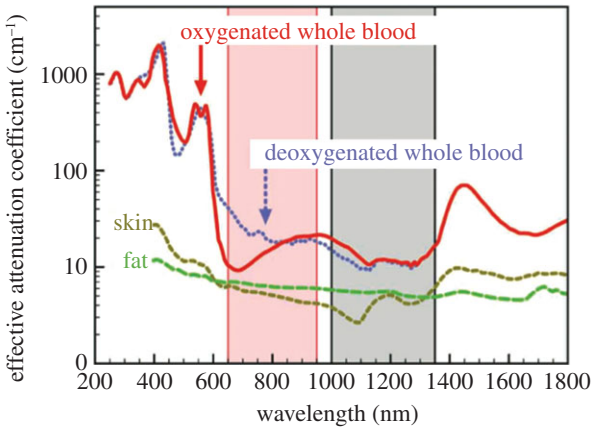

Figure 1. Absorption properties of various tissue components showing the windows in the near-infrared spectral region. (Adapted from Mitchell *et al.* [17] with permission from the Nature Publishing Group. Original figure provided by Dr Andrew Smith of Emory University.) (Online version in colour.)

While our laboratory has focused primarily on the delivery of the bioregulator diatomic molecules nitric oxide (NO) [1–3] and carbon monoxide (CO) [4,5] from metal complex precursors, it is clear from the theme of this Discussion Meeting Issue of *Philosophical Transactions A* that there is considerable interest in other chemotherapeutic applications of such photochemical strategies. Here, we will discuss some of the principles and potentially therapeutic applications of multi-photon excitation, then focus on developments concerned with the photochemical delivery of NO.

NO is endogenously produced in mammalian physiology and is an important mediator in numerous functions including cardiovascular control, neurotransmission and immune response [6]. Of special interest to our laboratory is the role that NO plays in sensitizing radiation damage to cellular tissue [7]. Malignant tumours have hypoxic regions that are more resistant to radiotherapy than are normoxic tissues; thus, it would be of interest to alleviate such resistance by releasing a radiation sensitizer and/or by vasodilation to increase oxygenation in the targeted tissues. NO can play both roles, the former requiring NO concentrations approaching 1 μM [7], the latter requiring nanomolar concentrations [8], both ranges being locally accessible by photochemical activation of an appropriate precursor.

NO is also known to trigger cell apoptosis (programmed cell death) [9], and this property offers another potential therapeutic application in cancer therapy [10]. However, NO plays contradictory roles in regulating apoptosis and has been implicated in both tumour growth and suppression as dictated by local concentrations [9,11–13]. For example, low [NO] stimulates angiogenesis (blood vessel growth) whereas the higher [NO] is inhibitory and promotes cell death [14]. Thus, if one chooses direct therapeutic NO application to kill tumour cells, it would be critical to ensure that a high dose is released at the target, given the dependence of cellular outcomes on NO concentrations and the potential for an unfavourable result. In this context, it is our view that the most effective application of NO release in cancer treatment will be in conjunction with radiotherapy or other chemotherapies that are enhanced by NO. Notably, the latter strategy depends strongly on being able to control the concentration and timing of NO delivery in order to maximize the synergism.

There are several properties of caged bioactive agents that are generally desirable for physiological applications. One is solubility in water or in a medium such as aqueous dimethylsulfoxide commonly used for intravenous drug delivery. It should be noted, however, that aqueous solubility is not an absolute requirement for local injection, and it may also be possible to implant a solid material incorporating the photochemical precursor. Thermal stability in aerated media at physiological temperatures is also highly desirable, so that the substance of interest is released only when triggered by light. A third key property, and the

one that is the principal focus of this article, would be photoactivity at excitation wavelengths where the transmission of light is optimal. The depth that excitation penetrates into tissue is strongly dependent on wavelength, transmission being optimal in the near-infrared (NIR) region [15–17]. The absorption profiles of various tissue components are shown in figure 1 [17]. According to these, light transmission through tissue would be the least for ultraviolet excitation wavelengths and become increasingly greater for longer visible wavelengths. The ideal windows for excitation would be at the NIR wavelengths. Historically the 'therapeutic window' was considered to be approximately 700–950 nm; however, the emergence of nanomaterial emitters and development of new detectors extend this range to 1300 nm. One way by which to utilize NIR wavelengths to access this window is by multi-photon excitation.

2. Some general comparisons between single- and multi-photon excitation

In order to lay the appropriate groundwork, we will briefly discuss some operational features of photochemical processes initiated by single-photon excitation (SPE), the typical case with most chromophores when excited with continuous light sources or even with lower intensity flashed sources having nanosecond or longer pulses. The response of chemical systems to SPE will then be compared with examples where multi-photon excitation plays a role, either by simultaneous absorption of two (or more) photons or by stepwise processes.

(a) Single-photon excitation

Different strategies have been pursued to cage the desired bioactive substance in a precursor that will be sensitive to the excitation wavelengths for which tissue transmission is feasible, even if not optimal. For example, we and others have worked to design molecular species and larger constructs that are photoactive for NO release at longer excitation wavelengths in the visible [10,18–20] and even in the NIR ranges [21]. However, doing so requires a compound that has appropriate absorption properties and reactivity when excited by longer wavelength light. In some cases, appropriately low energy electronic states capable of the desired uncaging process are potentially accessible, but direct excitations to these from the ground state are spin or symmetry forbidden.

An example would be the chromium(III) dinitrito complex *trans*-Cr(cyclam)$(ONO)_2^+$ ('CrONO'; cyclam = 1,4,8,11-tetrazacyclotetradecane) that has been studied in our laboratory as a photochemical precursor that releases NO reversibly (equation (2.1)) with a moderately large quantum yield at excitation wavelengths as long as 546 nm [22].

$$\textit{trans}\text{-Cr(cyclam)}(ONO)_2^+ \underset{k_{NO}}{\overset{h\nu}{\rightleftharpoons}} \textit{trans}\text{-Cr(cyclam)}(ONO)(O)^+ + NO \tag{2.1}$$

The reactive excited state (ES) has been identified as a doublet ligand field (LF) state with an energy of approximately 1.77 eV (approx. 700 nm). This can be populated by internal conversion/intersystem crossing from the higher energy states formed by excitation in the visible range as illustrated by the ES diagram shown in figure 2. Notably, direct excitation from the quartet ground state to the reactive doublet ES is both spin forbidden and symmetry (Laporte) forbidden [23], given that the parities of the ground and the LF ESs are the same, and that an allowed single-photon transition requires a dipole change. Furthermore, while the spin-allowed d → d transitions to the lower energy quartet LF ESs are in the visible (λ_{max} 470 nm), they too are Laporte forbidden in this centrosymmetric d^3 complex. Therefore, even these ^{4}[CrONO] → ^{4}[CrONO]* bands have small extinction coefficients ($\varepsilon_\lambda \sim 40\ M^{-1}\ cm^{-1}$) and thus are quite weak.

Why does this matter? The ability of a photochemical precursor to deliver a caged molecule will depend on a number of factors. Two important quantitative parameters are the *quantum yield* of the desired photoreaction and the *rate* of the photochemical uncaging of the bioactive substance of interest. For SPE, the quantity of the photoproduct (P) generated should be a linear function of

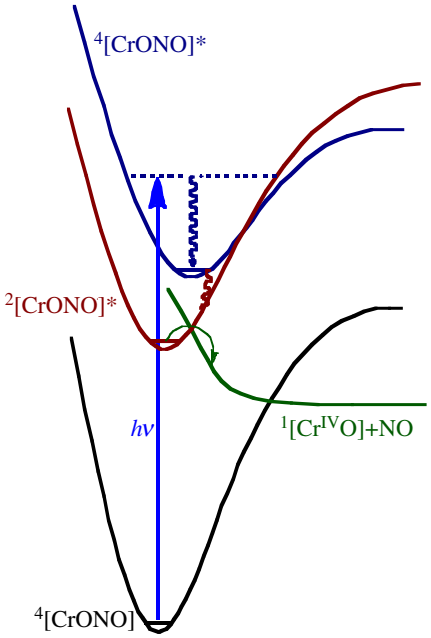

Figure 2. Hypothetical pathway for the photolabilization of NO from *trans*-Cr(cyclam)(ONO)$_2^+$ (CrONO). Single-photon excitation into the quartet excited state is followed by intersystem crossing to the doublet excited state from which NO is released. (Figure reproduced with permission from Ostrowski *et al.* [22]. Copyright the American Chemical Society.) (Online version in colour.)

the number of photons directly absorbed by the photoactive precursor; thus the quantum yield (Φ_P) is defined by

$$\Phi_P = \frac{\Delta P}{\Delta h\nu}, \tag{2.2}$$

where ΔP would be moles of product formed and $\Delta h\nu$ would be einsteins of light *absorbed* by the photoactive substance. Technically, the quantum yield should be determined for excitation at a specific wavelength, since Φ_I may be wavelength dependent.

The quantum yield can also be defined in terms of the photoreaction *rate:* d[P]/dt. The latter is a particularly important consideration when the goal is to affect a dynamical physiological system by photo-uncaging. For example, in solution one can write

$$\Phi_P = \frac{\mathrm{d[P]}/\mathrm{d}t}{I_a}, \tag{2.3}$$

where (d[P]/dt) is the rate of product formation in moles per unit volume per unit time and I_a is the intensity of the light absorbed[2] in einsteins per unit time per unit volume at the excitation wavelength (one einstein = 6.023×10^{23} photons). Thus, the rate of product formation would be

$$\frac{\mathrm{d[P]}}{\mathrm{d}t} = \Phi_P I_a. \tag{2.4}$$

I_a is a function both of the incident light intensity I_0 and of the ability of the compound to absorb at the wavelength of excitation. For a solution phase system where the photoreactant is the only

[2]Intensity can also be defined as energy per unit time per unit area when discussing a light beam (see below).

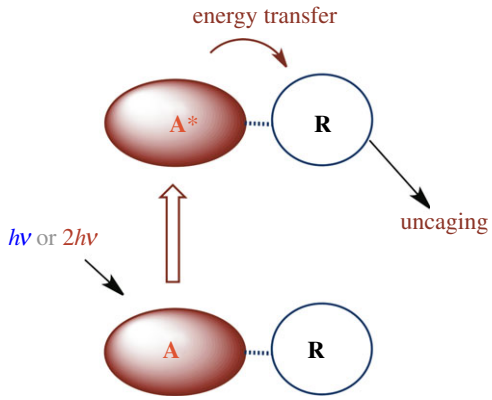

Scheme 1. A represents a strongly absorbing antenna, **R** represents the precursor to the bioactive substance that is uncaged once the appropriate ES of **R** is populated. (Online version in colour.)

species absorbing the incident light[3]

$$I_a = I_0(1 - 10^{-\mathrm{Abs}(\lambda)}). \tag{2.5}$$

Abs(λ) is the solution absorbance at the excitation wavelength λ_{irr} and equals the product of the molar concentration of the photoactive species (c), molar extinction coefficient $\varepsilon(\lambda)$ (in $\mathrm{l\,mol^{-1}\,cm^{-1}}$) and the pathlength of the solution cell (in cm). Thus, the rate of photoproduct formation under SPE at a particular wavelength will be directly proportional to I_0 and to Φ_P and will be a more complex function of c and $\varepsilon(\lambda)$. If the product of c and $\varepsilon(\lambda)$ is sufficiently large, all the light is absorbed and the photoreaction rate becomes independent of both terms, although this scenario is unlikely in a targeted tissue, as well as is the premise that the photoreactant is the only absorbing species. In this context, efficient photochemical delivery to physiological targets should be more favourable with precursors that absorb strongly at the desired excitation wavelength(s) λ_{ex}.

When polychromic light is used as the excitation source, the photochemical rate would be the integral of the product $\Phi_i I_a$ over the excitation wavelengths, noting that Φ_i may be and I_a certainly will be functions of λ_{irr}.

In order to obtain such photochemical precursors, it is often of interest to develop molecular constructs containing strongly absorbing chromophores that can act as antennas to capture desirable wavelengths of light (scheme 1). If the ESs of these antennas are energetically capable of internal energy transfer to the ES capable of the desired reaction (conservation of energy must be obeyed), then the larger SPE absorption cross sections of the antennas can lead to greatly enhanced rates of uncaging. In simple terms, the rates of the photosensitized reaction will be equal to

$$\left(\frac{\mathrm{d[P]}}{\mathrm{d}t}\right) = \Phi_P I_a(\mathbf{R}) + \Phi_{EN}\Phi_P I_a(\mathbf{A}), \tag{2.6}$$

where Φ_P is the quantum yield for the uncaging reaction from the ES of the precursor **R**, $I_a(\mathbf{R})$ is the intensity of light absorbed directly by **R**, Φ_{EN} is the efficiency of energy transfer from $\mathbf{A}^*$ to **R**, and $I_a(\mathbf{A})$ is the intensity of light absorbed by the antenna **A** at the excitation wavelength. Thus, if the product $\Phi_{EN} I_a(\mathbf{A})$ is larger than $I_a(\mathbf{R})$, substantial enhancement of the photoreaction would ensue from the antenna effect.

[3]When other absorbing species are present, such as the developing reaction photoproducts, corrections need to be introduced for such inner filter effects.

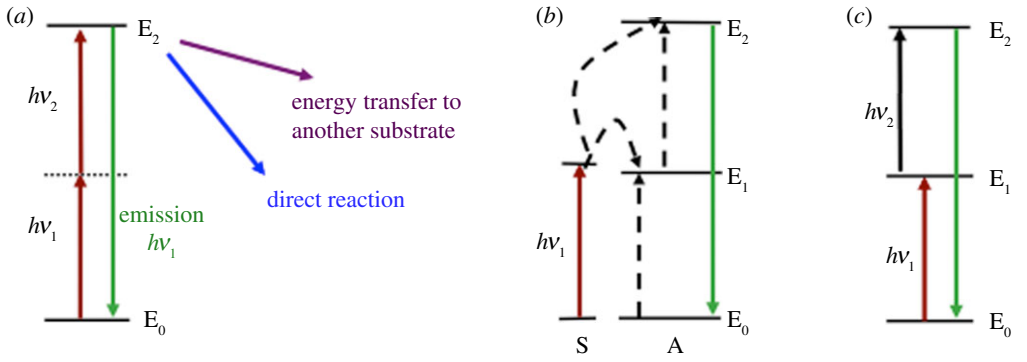

Scheme 2. Three simplified models for multi-photon excitation. (*a*) TPE involves the simultaneous absorption of two photons, usually, but not necessarily, of the same energy. The excited state formed may undergo emission, direct reaction to product or energy transfer to another substrate. (*b*) In the ETU model shown, the single-photon excitation of sensitizer component (S) gives an excited state that can sensitize an acceptor (or 'activator', if emissive) component (A) having a long-lived ES E_1 (the shorter curved dashed line). Further excitation of the sensitizer S results in additional energy transfer from S* to A* to give the higher energy ES E_2 (the longer curved dashed line) from which emission may occur. (*c*) Excited state absorption differs from the first two in that the higher energy ES is formed by sequential direct absorption of photons by a single molecular component. (Online version in colour.)

In this context, studies in our laboratory have shown that both organic dyes and quantum dots (QDs) can act as effective antennas for the photosensitization of NO release from *trans*-Cr(cyclam)$(ONO)_2^+$ [24,25] thereby increasing, in each case, the photochemical rate of the reaction depicted in equation (2.1).

(b) Multi-photon excitation

The reactive ESs of many otherwise attractive precursors are not low enough in energy to be accessed by SPE of an antenna with strong absorption bands at longer visible wavelengths or in the NIR therapeutic window. This led our laboratory to consider a different approach, namely, multi-photon excitation, where the additive energy of two or more NIR photons would be sufficient to generate the desired precursor state for uncaging. Two types of multi-photon excitation will be addressed in the discussion below: (a) simultaneous absorption of two quanta of light (two-photon excitation or TPE) and (b) NIR-to-visible/UV energy transfer upconversion (ETU) involving sequential absorption processes (see scheme 2). Multi-photon excitation, whether by simultaneous or sequential processes, will typically have a nonlinear dependence of the photoreaction rate upon I_0, and this behaviour is very different from that noted above for SPE stimulated processes (equation (2.4)).

Simultaneous two-photon absorption processes were first discussed in the 1930s by Maria Goeppert-Mayer (after whom GM, the units of two-photon absorption, are named), but experimental verification of these ideas occurred decades later [26]. The primary reason for the lengthy delay was that the high monochromatic light intensities necessary to test the concept were not routinely accessible until the advent of lasers, since the probability of TPE is proportional to I^2, the square of the light intensity, if a single light source is used.[4] This quadratic relationship means that the probability of TPE is highest at the focal plane of a focused light source (see figure 3).

[4]Notably, simultaneous two-photon absorption does not require that both photons are of the same frequency; however, for simplicity, we will restrict our discussion to the case where there is a single, high intensity light source functioning at a single frequency.

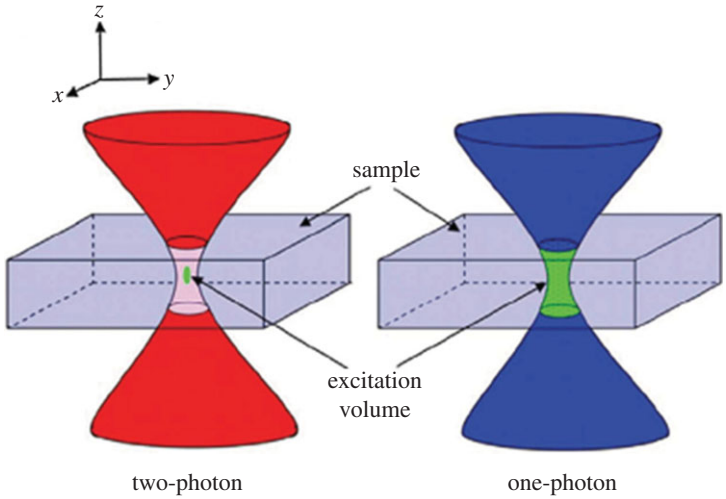

Figure 3. Illustrations of the excitation volumes resulting from SPE and TPE processes occurring with a focused beam of light. Since the units of *I* are einsteins per unit time *per unit volume*, a focused beam will have the highest intensity at the focal point in a non-absorbing medium. (One can also define intensity in terms of energy per unit time per unit area. A typical Ti/sapphire ultrafast laser operating at pulse frequency, energy and length of 80 MHz, 6 nJ and 100 fs, respectively, with a beam diameter of 120 μm translates into average pulse intensities of approximately 5×10^8 W cm^{-2}.) In a weakly absorbing medium, the highest rate of single-photon absorption would also be at the focal point, although this would be proportional to r^{-2} (where r is the radius of the beam at a particular point along the propagation axis z). However, in a strongly absorbing medium, I would be attenuated as a function of z beginning at the surface of the sample. With TPE, I^2 is proportional to r^{-4} and hence is much more sensitive to the position of the focal plane along z. (Adapted from Pedersen *et al.* [27], with permission from Informa Healthcare.) (Online version in colour.)

This confers three-dimensional spatial resolution to the excitation profile, a property that has been extensively exploited in biological imaging [28,29] and offers some very interesting possibilities in photochemical therapy [27,30].

The theory of two-photon excitation (absorption) is presented in greater detail elsewhere, so our focus here will just be on several key features that characterize TPE processes to provide a possible guideline regarding potential applications of this technique. When a beam of monochromatic light with wavelength λ propagates through an optical medium, its intensity is attenuated according to

$$\frac{\mathrm{d}I(x)}{\mathrm{d}t} = -\alpha(\lambda)I(x) - \beta(\lambda)I(x)^2 - \gamma(\lambda)I(x)^3 - \ldots, \tag{2.7}$$

where $I(x)$ is the transverse light intensity at any point x. The first term corresponds to typical SPE, while the subsequent and progressively weaker terms correspond to two- and three-photon absorption, etc. Conservation of energy is also required for any resonant transition. Therefore, with TPE, $E_\mathrm{f} - E_\mathrm{i} = 2h\nu$, where $E_\mathrm{f} - E_\mathrm{i}$ is the energy difference between the initial and final states. The selection rules for TPE are different from those for SPE, in particular, the former is allowed only between two states that have the same parity, while the latter requires a change in parity. Thus, in a centrosymmetric molecule, an allowed one-photon transition from the ground state to a given ES would not be two-photon allowed and vice versa, although mixing with appropriate vibronic terms can increase the allowedness of specific electronic transitions. Of course, for molecules without an inversion centre, transitions can be both single-photon and two-photon allowed.

There have been considerable experimental efforts to define the types of chromophores that have high TPE cross sections [28]. Among these, organic π-conjugated ones are attractive for TPE applications in the NIR, since SPE transitions in this region are typically forbidden by

conservation of energy considerations. The 2008 review by He and co-workers [26] describes a number of effective TPE chromophores and offers some general guidelines for designing such species. For example, it is argued that species with intramolecular charge transfers, that is, molecules with both electron-rich π-donor and electron-demanding π-acceptor components and extended conjugation will be active two-photon absorbing chromophores. The evolution of such structure/activity design considerations has also pointed to π-conjugated quadrupolar molecules with such electron-donor and -acceptor units arranged symmetrically with respect to the centre of the molecule as having large two-photon cross sections in the NIR region [31]. This has led to a sizable effort into the development of new TPE chromophores [26,31,32], although as He and co-workers [26] pointed out, there is some difficulty in comparing the quantitative two-photon absorption cross-section values reported, since these have been measured by different techniques and under different conditions.

Various types of nanoparticles constitute another class of TPE chromophore and there is a growing interest in developing different multi-photon driven systems using such materials as antennas for excitation with NIR light [33,34]. For example, two-photon absorption cross sections as large as 10^4 GM ($1\,\mathrm{GM} = 10^{-50}\,\mathrm{cm}^4\,\mathrm{s\,photon}^{-1}$) are commonly observed with semiconductor QDs such as the cadmium selenide core or CdSe/ZnS core/shell QDs, and the magnitude increases dramatically as the size of the cores increases [35,36]. A detailed discussion of the biological applications of nanomaterials under multi-photon excitation is outside the intended scope of this article.

3. Some therapeutic applications of two-photon excitation

Imaging and microscopy comprise by far the most extensive applications of multi-photon excitation in biology [28,29,37]. A medical application is in photodynamic therapy (PDT), a method involving the excitation of a sensitizer, followed by energy transfer to dioxygen (O_2) leading to the formation of singlet dioxygen (scheme 3), which has the capability to destroy diseased tissue (or in some cases, pathogens) at that site [38–40]. The triplet ground state of O_2 has the $^3\Sigma_g^-$ electronic configuration and direct excitation to the singlet $^1\Delta_g$ state (approx. 1270 nm) is forbidden, so an indirect approach via photosensitization is necessary for the latter's preparation. Notably, such energy transfer occurs from the sensitizer triplet state T_1 that is formed by intersystem crossing from the singlet ES formed by direct excitation. For this reason, the effectiveness of the sensitizer is dependent on the efficiency of the intersystem crossing, so features such as heavy atoms are often incorporated into the sensitizer to enhance the rate of this process relative to those of the competing radiative and non-radiative deactivation of the S_1 state.

The S_1 ES can be formed by SPE or TPE. The advantage of SPE is that it is generally much more efficient, so in order to take advantage of the therapeutic window, a variety of sensitizers, such as various porphyrins, phthalocyanines and other polypyrrole macrocycle derivatives that absorb at longer visible wavelengths (600–800 nm) have been prepared and tested for their efficacy in PDT applications [40]. Other desirable properties include aqueous solubility, dark stability in aerobic media, selectivity of uptake and retention by the targeted cells and the absence of significant toxicity to the host.

Applications of TPE to PDT again have been directed towards taking advantage of the tissue transmission properties of NIR light and the spatial resolution provided by the quadratic dependence on the intensity of the exciting light [27,39,41]. The latter has been demonstrated *in vivo* by using TPE and PDT dyes to seal blood vessels in mice [42]. Nonetheless, there is some concern about the difficulty of achieving appropriate focusing of lasers given the scattering inherent to a nonhomogeneous material such as mammalian tissue.

The three-dimensional resolution opportunities provided by TPE have extensively been exploited in neuroscience both in tissue samples and *in vivo* [43–50]. The NIR TPE induced uncaging of neurotransmitters such as glutamate (figure 4) and has allowed the functional mapping of the respective receptors in neurons with high-resolution (μm), sub-cellular precision

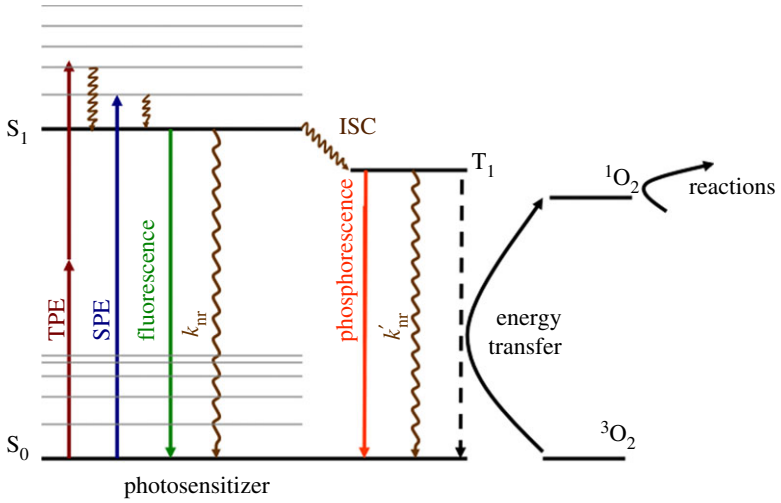

Scheme 3. Generic energy level diagram showing spin-allowed excitation of a sensitizer to the S_1 excited state followed by intersystem crossing (ISC) to the T_1 triplet state in competition with fluorescence and non-radiatiative decay (k_{nr}). The T_1 state can itself undergo unimolecular spin forbidden radiative emission (phosphorescence) or non-radiative decay (k'_{nr}) in competition with bimolecular energy transfer to ground state $^3O_2$. (Online version in colour.)

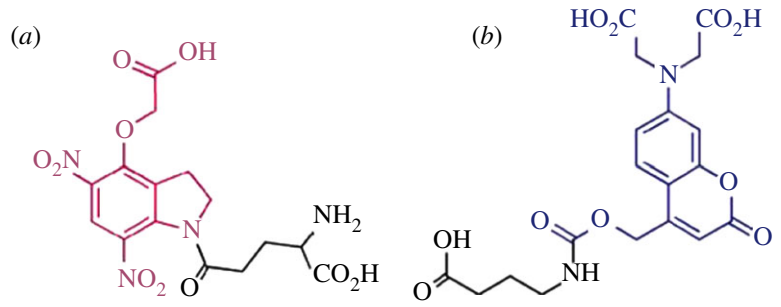

Figure 4. Examples of compounds that are photochemical precursors ('caged') of the neurotransmitters glutamic acid (*a*) and γ-aminobutanoic acid (*b*). For (*a*) the photoactive chromophore is a 4-carboxymethoxy-5,7-dinitroindolinyl derivative, while for (*b*) it is a 7-aminocoumarin derivative. These are active towards release of the respective neurotransmitter upon two-photon excitation at 720 and 830 nm, respectively [47]. (Online version in colour.)

[48]. The species shown in figure 4 use π-unsaturated aromatic compounds as the TPE chromophores, but it should be noted that metal complexes such as ruthenium amines have similarly been used as chromophores for TPE uncaging of neurotransmitters [46,51].

TPE has also been recently explored as a possible methodology for the targeted uncaging of cancer chemotherapy drugs [52–54] and antibacterials [54] as well as for ophthalmologic applications [55]. In one such example [54], the drugs of interest were encapsulated in water soluble micelles of a biocompatible block copolymer of poly(ethylene oxide) and a poly(L-glutamic acid) derivatized with coumarin dyes. TPE of these materials using 794 nm light led to dissociation of the dyes from the polypeptide and a shift of the hydrophilic–hydrophobic balance and destabilization of the micelles, leading in turn to release of the encapsulated drugs.

4. Two-photon excitation in NO delivery

Our personal interest in TPE began with iron/sulfur/nitrosyl clusters known as Roussin's red salt esters (RSEs) that have the general formula $Fe_2(NO)_4(\mu\text{-}SR)_2$, where the substituent R on the

bridging thiolate may be a simple alkyl or aryl group or a more complex chromophore. Upon excitation with near-UV or shorter visible wavelengths, RSEs are quite photoactive in solution with initial excitation leading to reversible NO release (equation (4.1), $k_{NO} = 1.1 \times 10^9\ M^{-1}\ s^{-1}$ in 295 K aqueous solution for $R = -CH_2CH_2SO_3^-$) [56].

$$Fe_2(\mu\text{-}SR)_2(NO)_4 \xrightleftharpoons[k_{NO}]{h\nu} Fe_2(\mu\text{-}SR)_2(NO)_3 + NO \tag{4.1}$$

In aerobic solution, the $Fe_2(NO)_3(\mu\text{-}SR)_2$ intermediate undergoes fast oxidative trapping by O_2 ($k_{O_2} \approx 1.1 \times 10^9\ M^{-1}\ s^{-1}$), the overall reaction leading to the release of all four NO's and oxidation of the iron to Fe^{2+}.

Thus, by varying the R-groups, it should be possible to incorporate desired optical or biological properties into the RSEs. In this context, Conrado *et al.* [18] in this laboratory prepared an RSE with a pendant protoporphyrin IX derivative **PPIX-RSE** which was shown to have significantly enhanced rates of NO production at longer visible-range λ_{irr} (e.g. 546 nm), relative to a simpler RSE such as $Fe_2(NO)_4(\mu\text{-}SEt)_2$. They concluded that **PPIX-RSE** works much like the illustration in scheme 1, where the pendant chromophore absorbs the exciting light, followed by energy transfer to the iron cluster and uncaging of NO. The enhanced rate of NO production can be attributed entirely to the antenna effect where the PPIX strongly increases $I_a(A)$, the intensity of the light absorbed by the antenna, since the net quantum yield actually decreased.

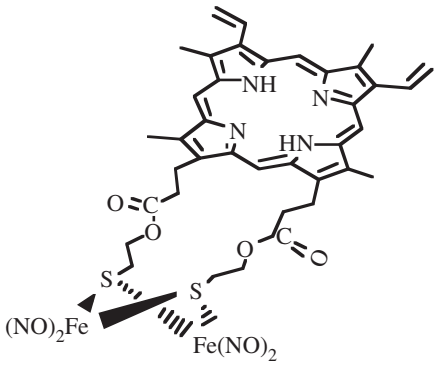

PPIX-RSE

Although the emission spectrum of **PPIX-RSE** is analogous to those of PPIX and its dimethyl ester **PPIX-DME**, the emission intensity from **PPIX-RSE** is strongly attenuated (approx. 90%). This quenching was probably due to energy transfer from the PPIX to the Fe cluster and was also reflected in markedly shorter luminescence lifetimes of that chromophore in **PPIX-RSE** as probed by ultrafast pulsed laser studies [18]. The dual lifetimes observed ($\tau_1 = 0.22$ ns, $\tau_2 = 10.7$ ns) suggested that two **PPIX-RSE** conformers were present, one much more readily quenched than the other, and this suggestion was confirmed by ion-mobility mass spectrophotometry experiments that detected both folded and open forms of this structure [57].

The question remained regarding whether TPE of such a chromophores would display a similar antenna effect and TPE stimulated NO release. Wecksler initiated this approach by subjecting a solution of **PPIX-RSE** to 810 nm NIR excitation with 100 fs pulses from a Ti/sapphire laser [58]. Despite the relatively poor two-photon absorption cross section (δ) of PPIX ($\delta = 2$ GM at 790 nm [59]), he found that this led to a weak emission from **PPIX-RSE** with a λ_{max} of 632 nm. Furthermore, NO was also generated. For comparison, TPE of PPIX or **PPIX-DME** under analogous condition gave much stronger emission, so the behaviour upon two-photon absorption paralleled that seen under SPE at much shorter λ_{irr}.

Wecksler extended these studies by preparing several other $Fe_2(NO)_4(\mu\text{-}SR)_2$ derivatives with chromophores known to have significantly higher δ values and carried out quantitative photophysical and photoreaction studies of these under both SPE and TPE. The depicted RSEs are **Fluor-RSE**, where the two pendant ligands are derived from the strongly luminescent dye fluorescein [60], and **AFX-RSE**, where the pendant chromophore(s) is a dye designed for TPE properties and prepared by the US Air Force Research Laboratory of Dr L.-S. Tan [61]. For both RSEs, the fluorescence properties of the ES species formed after TPE at 800 nm were equivalent to those of the ES formed upon SPE at much shorter wavelengths (436 nm). Thus, it appears that the same ligand-centred singlet states are formed regardless of the method of excitation. Furthermore, in each case, the fluorescence was markedly attenuated from that of analogous chromophore models without the Fe/S/NO cluster, and this was accompanied by shorter fluorescence lifetimes and NO release. These observations are qualitatively consistent with an energy transfer mechanism from the excited PPIX chromophores to the metal clusters.

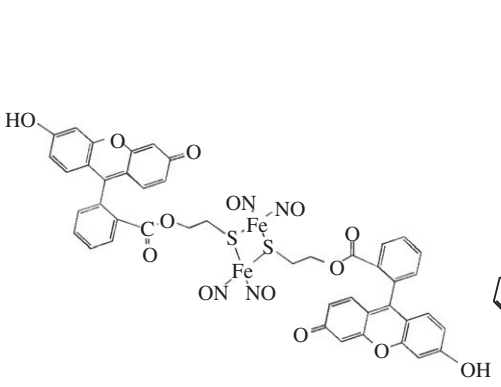

Fluor-RSE

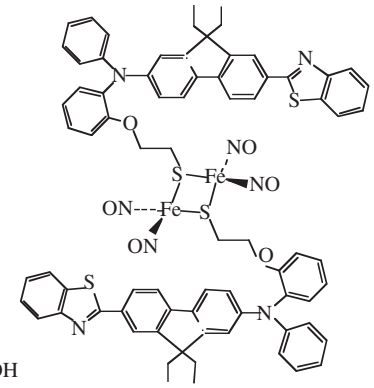

AFX-RSE

The quantitative emission properties of **Fluor-RSE** and **AFX-RSE** upon TPE were used to determine the two-photon absorption cross section δ according to equation (4.2):

$$\delta = \frac{\Phi_{\text{ref}}\delta_{\text{ref}}c_{\text{ref}}P_{\text{ref}}^2 I}{\Phi c P^2 I_{\text{ref}}} K. \tag{4.2}$$

In this treatment, I is the integrated fluorescence intensity, c the concentration, Φ the fluorescence quantum yield, P the excitation power, K the solution refractive index ratio and ref designates the reference. Fluorescein ($\delta = 38$ GM at 782 nm at pH 11 [62]) was used as the reference, and given that the conditions for measuring the sample and reference were identical, we can assume that $P = P_{\text{ref}}$ and $K = 1$. In this manner δ was determined to be 63 ± 5 GM for **Fluor-RSE** [60] and 246 ± 8 GM for **AFX-RSE** [61]. Furthermore, the NO release was measured using a NO-specific electrode. For excitation of *Fluor-RSE* with 800 nm light, a log/log plot of the NO generated versus the excitation intensity proved to be linear and had a slope of 1.8 ± 0.2 [60]. Thus, the rate of NO production is (within experimental uncertainty) proportional to the square of the intensity of the exciting light as would be predicted for a TPE mechanism (scheme 2).

In a subsequent study, Prasad and co-workers [63] prepared another RSE derivative $Fe_2(NO)_4(\mu\text{-}SR')_2$, where R′ (see formula) is the conjugate of an oligo-phenylene vinylene amine, which serves as the TPE chromophore, and three tetra(ethylene glycol) monomethyl ether units

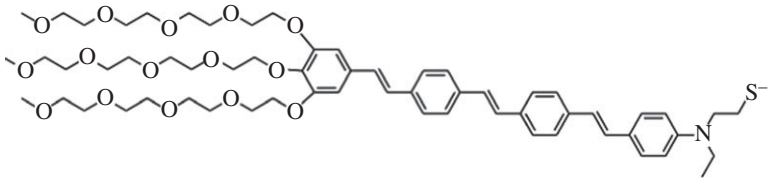

R'S⁻

to improve aqueous solubility. Again the emission from the chromophore ($\lambda_{max}^{em} = 544$ nm) was largely quenched as the result of energy transfer to the di-iron cluster. The two-photon absorption cross section of this complex was determined to be 682 GM at 775 nm. Both SPE at 365 nm and TPE at 775 nm led to NO release which was detected by electron paramagnetic resonance (EPR) spectroscopy using $Fe(MGD)_2$ (MGB = *N*-methyl-D-glucamine dithiocarbamate) as a trapping agent to give the EPR active $Fe(MGD)_2(NO)$ [64]. Since the fluorescent ligand was also released from the metal cluster as the result of the photolabilization of NO followed by oxidative secondary reactions, as previously seen with **PPIX-RSE** and **Fluor-RSE** [18,60], the net fluorescence from the solution increased as the photoreaction progressed. These workers also demonstrated using both HeLa and Cos-7 cancer cell cultures that the NO release generated by either SPE or TPE of $Fe_2(NO)_4(\mu\text{-}SR')_2$ led to light-dependent cytotoxicity, although the magnitude of the effect was greater in the SPE experiments owing to the greater flux of NO generated with direct UV excitation.

The interest in TPE-facilitated delivery of NO using NIR light has also stimulated some recent interest in organic photochemical precursors. Miyata and co-workers [65] have reported a novel 2,6-dimethylnitrobenzene based NO donor that is linked to a fluorescein as the two-photon absorbing moiety and therefore does not contain metal ions. This new species, **Flu-DNB**,

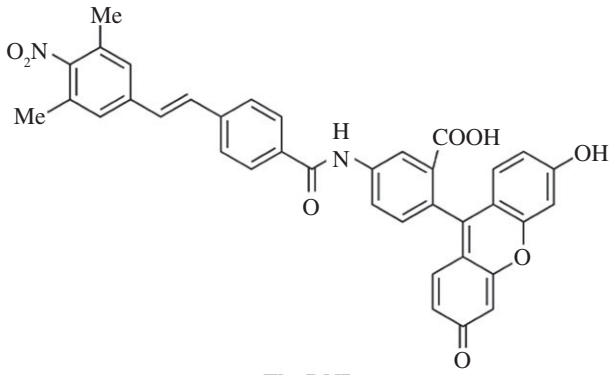

Flu-DNB

releases NO when excited with 330–380 nm (UV-A) light, as demonstrated by trapping with $Fe(MGD)_2$ to give the EPR active adduct $Fe(MGD)_2(NO)$. Similarly, **Flu-DNB** is photoactive when subjected to pulsed excitation with an ultrafast laser at 720 nm where the system does not demonstrate single-photon absorption, and thus a TPE process is indicated. Uncaging of NO was also detected under the latter conditions, although the overall two-photon uncaging cross section was quite small (less than 1 GM). Notably, the uncaging cross section is a product of the two-photon absorption cross section and the quantum yield for NO release from the ES formed by TPE. Since uncaging was not observed upon irradiation of **Flu-DNB** at 450–480 nm, the λ_{max} of the fluorescein chromophore, it appears probable that NO release is occurring from higher energy ESs that are only inefficiently populated by the TPE process in this case. Subsequently, the same group has reported several other nitrobenzene derivatives that release NO under NIR TPE; however, the uncaging cross sections are low in each case [66].

5. Uncaging using upconversion nanoparticles

(a) Introduction to Ln^{III}-doped upconverting materials

Upconversion is a nonlinear process that involves the sequential absorption of multiple photons via long-lived ESs followed by emission at higher energy than the excitation source. For example, NIR excitation may result in UV, visible or NIR emission [67]. Phosphors based on the lanthanoid ions can be effective upconversion devices owing to the relatively long lifetimes of their f–f states. The electronic spectroscopy of the Ln^{III} ions is largely determined by the shielding of the partially filled 4f orbitals by the filled $5s^2$ and $5p^6$ electron sub-shells. As a consequence, the energies of

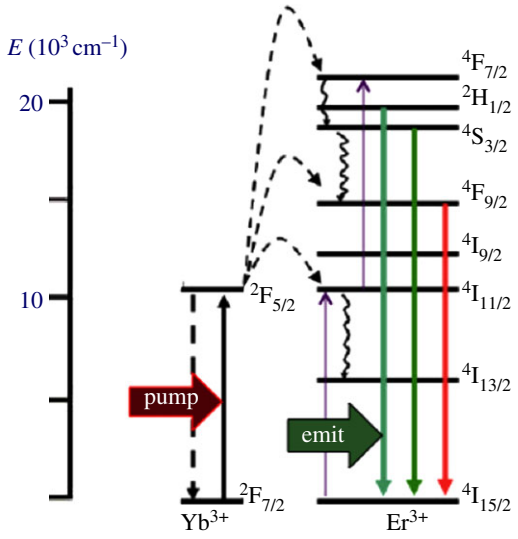

Figure 5. Illustration of the upconversion process for a UCNP where the sensitzer ion is Yb^{3+} and the activator ion is Er^{3+}. Pumping the sensitizer with 980 nm NIR light results in several visible-range emissions, the absolute and relative intensities of which depend nonlinearly on the intensity of the pumping process. Because of the shielding of the 4f orbitals (by the filled 5s and 5p sub-shells) and the forbidden nature of the f $\rightarrow$ f transitions in Ln^{3+} ions, the excited states are long-lived. Excitation of the sensitizer Yb^{3+} populates its $^2F_{5/2}$ state (the 'pump' mechanism). Energy transfer from the $Yb^{3+}{}^2F_{5/2}$ state to the Er^{3+} activator gives the $Er^{3+}{}^4I_{11/2}$ state, which is relatively long-lived although it does slowly decay to the $Er^{3+}{}^4I_{11/2}$ state. Further pumping of the $Yb^{3+}{}^2F_{7/2}$ —^{2} $F_{5/2}$ transition is followed by energy transfer to the excited activator, a process (sequential energy transfer) that combined with internal relaxations (wavy lines) gives upconverted higher energy levels of Er^{3+} ($^4F_{7/2}$, $^4S_{3/2}$ and $^4F_{9/2}$) from which emission is observed. In this manner, the activator may release its stored energy as photons of higher energy than the excitation source. Adapted from Zhang *et al.* [79]. (Online version in colour.)

4f–4f electronic transitions are primarily defined by spin and electronic repulsion terms and show little sensitivity to the chemical environments of the Ln^{III} ions whether in solution or diluted in a solid [68]. Altogether, this produces well-defined 4f electronic energy levels and relatively sharp absorption and emission bands, although 4f–4f transitions are parity forbidden. The lifetimes of 4f–4f ESs are more sensitive to the environment, since collisional pathways and vibronic coupling can contribute dramatically to non-radiative deactivation. Incorporating such ions in a solid matrix eliminates collisional contributions while the choice of the appropriate matrix can suppress phonon-coupling pathways important to non-radiative deactivation. Thus, doping Ln^{3+} cations into a sodium yttrium fluoride matrix $NaYF_4$, especially one in the β-phase, leads to strong emissions from the f–f states of these ions owing to the longer lifetimes under such circumstances. These properties are especially well suited for the NIR to UV/visible upconversion nanoparticles (UCNPs) [69–72] that will be discussed in this section.

Upconversion commonly occurs by ETU or ES absorption mechanisms (scheme 2). Other less common pathways are photon avalanche [67], cooperative sensitization and cooperative luminescence [73–77]. Once termed APTE (addition de photon par transfert d'energie) [78], ETU uses sequential energy transfers from a sensitizer to an activator. For a Ln^{III}-doped UCNP, the sensitizer is an ion such as ytterbium(III) in the crystal lattice that absorbs the excitation photon, temporarily stores the energy in a metastable level and then transfers it to an activator ion such as europium(III), terbium(III) or thulium(III) to form a metastable ES of the latter. Subsequent energy transfer from a sensitizer ion to the already excited activator ion produces new, higher energy states that can undergo emission as the result of 'upconversion'. The resulting emission (or emissions), which is the consequence of sequential multi-photon processes, occurs at a higher energy than the initial excitation source, as illustrated in figure 5 for a system with Yb^{3+} as the sensitizer ion and Er^{3+} as the activator ion [79].

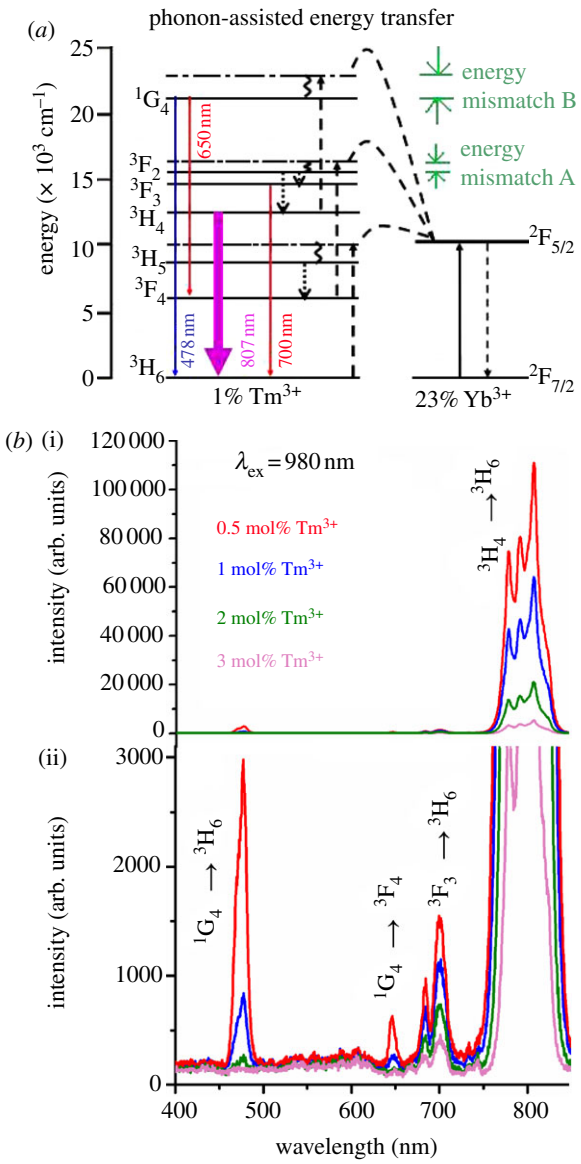

Figure 6. (*a*) When Yb^{3+} is used as the sensitizer, irradiation at 980 nm provides the excitation energy. The upconversion mechanism is shown including energy mismatches for the Yb^{3+} ($^2F_{7/2} \rightarrow {}^2F_{5/2}$) to the Tm^{3+} ($^3H_6 \rightarrow {}^3H_5$, $^3F_4 \rightarrow {}^3F_2$ and $^3H_4 \rightarrow {}^1G_4$) energy levels. Solid arrows represent photon absorption or emission, dotted arrows represent multi-phonon relaxation, dashed arrows represent phonon assisted energy transfer, and wavy arrows represent energy mismatches. Note that all of the emission lines shown (478, 650, 700 and 807 nm) occur at higher energy than the 980 nm excitation source. For this particular material (GaF_3 matrix) the NIR 807 nm emission line is by far the strongest emission. (*b*) (i) The upconversion spectrum of UCNPs excited at 980 nm (90 mW), consisting of 23% Yb^{3+} and 0.5–3 mol% Tm^{3+} in a GdF_3 matrix. (ii) Vertical axis is magnified to show the details of the visible emission spectra. (From Wong *et al.* [80]. Reproduced with permission from the Optical Society). (Online version in colour.)

With ETU, energy transfers to neighbouring ions are often between states that are not exact matches; that is, the transition involves excess or insufficient energy mismatch as illustrated in figure 6 [80]. In the former case, the excess energy may result in phonon release, while the opposite would be required for the latter case. Figure 6 also illustrates a case where the solid matrix has

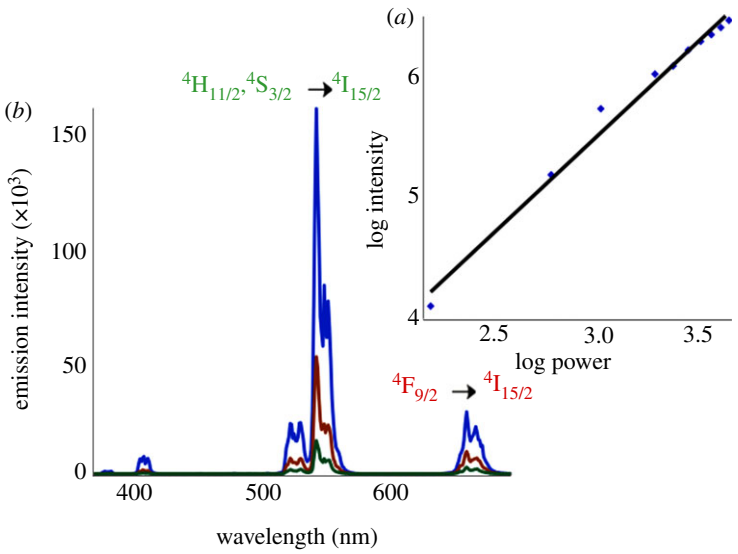

Figure 7. (*a*) Log/log plot of emission intensity at 550 nm versus power of the excitation laser. This shows the nonlinear response of emission intensity to excitation power, giving a slope of 1.63 (J. V. Garcia, studies in progress). (*b*) Upconversion visible-range emission spectra of an aqueous suspension of silica coated β-$NaYF_4$:Yb/Er (20/2%)@$NaYF_4$ core:shell UCNPs at three different powers of the 980 diode laser (0.58, 0.96 and 1.36 W). (Online version in colour.)

been chosen such that the upconverted NIR emission at approximately 805 nm is favoured over visible emission.

Ln^{III}-doped UCNPs incorporate the sensitizer and activator ions in a host crystal lattice, such as $NaGdF_4$, $NaYF_4$, $LaPO_4$, YF_3 or Y_2O_3 [81–85]. Of these, the β-phase (hexagonal) $NaYF_4$ host lattice has particularly favourable properties [86]. Using a $NaY(Gd)F_4$ host lattice, one can prepare hexagonal phase and small (approx. 10 nm diameter) UCNPs [86–88]; however, the small particle size increases solvent quenching, especially by OH and NH groups, owing to the sizable percentage of the lanthanoid emitters that are at or near the surface in such species. Such quenching may be reduced by growing a shell of unsubstituted host material around the UCNP [89,90] to isolate surface ions from these environmental effects. Related modifications of UCNPs include silica or polymer coatings [91–98]. The former increase aqueous solubility (provided the particles are small enough) and bonding with peptides, siRNA, dyes or other organic molecules [99]. Notably, the sharp emission lines (10–20 nm at full width at half maximum) and long-lived ESs simplify emission detection in imaging applications. Furthermore, UCNPs are also quite photostable and show no bleaching even after hours of excitation.

In terms of the photophysical properties, it should be noted that the upconversion efficiency of a UCNP sample will be markedly power dependent owing to the nonlinear nature of this process. An example from this laboratory is noted in figure 7, which demonstrates a linear log/log plot of emission intensity at 550 nm from an aqueous sample of silica coated $NaYF_4$:Yb/Er (20/2%) UCNPs versus the power reading of a continuous wave (CW) diode laser operating at 980 nm with a beam diameter of about 2 mm. Given the slope of this plot (1.63), the nonlinear response of the emission brightness to excitation intensity is obvious. A higher energy luminescence that requires more than two 980 nm photons to populate could easily show a higher-order dependence on the laser power. At sufficiently high intensity excitation, the power dependence of the emission should saturate since the sensitizer population should reach a steady state at high light flux, and maximum emission quantum yields would be observed under such conditions. Although high upconversion efficiencies have been reported in one case for a solid Ln^{III}-doped material [100], most workers have found much lower values and this would be expected with potential physiological applications. For example, Boyer & van Veggel [101] used an integrating sphere to

measure quantum yields for the green emission from the upconversion material $NaYF_4$: Yb/Er (20/2%) and reported a value of 3 per cent for such powders using a power density of 20 W cm^{-2}, which is consistent with earlier studies by Page *et al.* [102]. Quantum yields for a colloidal suspension of core:shell UCNPs (approx. 30 nm diameter) in hexanes were an order of magnitude lower (0.3%) despite the use of an excitation intensity (150 W cm^{-2}) near the saturation of the power dependence curve. Even smaller quantum yields were observed in the absence of the $NaYF_4$ shell [101], thus pointing to the value of such shells with small nanoparticles.

(b) Several biological applications of upconversion nanoparticles

NIR upconversion fluorescence imaging reduces photo-damage to living cells and tissues, and is accompanied by very low autofluorescence background, decreased light scattering and high detection sensitivity as well as the greater light penetration depth of the excitation light in biological tissues. As noted above, the narrow line luminescence, long ES lifetimes and photostability of Ln^{III}-doped UCNPs make these particularly well suited for biological imaging. In this context, there have been some really exciting developments in cellular imaging [103–107] and *in vivo* imaging with small animals [103,104,108–111]. For example, strongly fluorescent core : shell β-$NaYF_4$:Yb,Er UCNPs, coated with a thin layer of SiO_2 and modified with amino groups, were covalently linked to rabbit anti-CEA8 antibodies. These were then used as fluorescent labels sensitive to NIR excitation to detect the antigen CEA, which is a cancer biomarker expressed on the surface of HeLa cells [105]. In another example, Nyk *et al.* [104] used NIR-to-NIR upconversion to achieve deeper tissue imaging using aqueous dispersible fluoride $NaYF_4$:Yb/Tm UCNPs (20–30 nm). *In vitro* cellular uptake was seen and whole body small animal (mouse) fluorescence imaging was demonstrated using a commercial Maestro GNIR FLEX system. No apparent cytotoxicity was found. Subsequent long-term studies by Xiong *et al.* [111] of whole body imaging with polyacrylic acid-coated $NaYF_4$:Yb/Tm UCNPs were able to track the biodistribution and excretion of the rare earth phosphors in mice. This study showed that injections of 15 mg kg^{-1} of these UCNPs led to no adverse effects on the health of the mice. These and other *in vivo* imaging studies, which have been recently reviewed [112], also indicate that UCNPs may prove useful for therapeutic applications with minimal toxicity.

One potential therapeutic application of UCNPs is PDT [113–117]. Ln^{III}-doped UCNPs have been explored as the initial chromophore in a multi-photon sequence of events leading to singlet oxygen generation for destroying diseased tissue or pathogens. The basic theme is the use of these non-toxic materials to absorb tissue transmitting NIR light. The upconverted emission is reabsorbed by organic dyes localized on the nanoparticle surface. Intersystem crossing gives the triplet states of these dyes appropriate for sensitizing the $^3\Sigma_g$ to $^1\Delta_g$ conversion of O_2 as illustrated in scheme 3. For example, UCNPs composed of $NaYF_4$ nanocrystal cores with a mesoporous silica shell (90 nm total diameter) loaded with the photosensitizer Zn(II) phthalocyanine were studied for their PDT effect on murine bladder cancer cells [113]. Intracellular uptake revealed a time- and concentration-dependent accumulation of these nanoparticles. Irradiation at 980 nm resulted in cytotoxic effects from the singlet O_2 generated. In another recent study, the effect of PDT triggered by 980 nm excitation of $NaYF_4$:Yb/Er UCNPs with Zn(II) phthalocyanine on the surface was shown to be effective in inactivating viruses [116]. Potential uses of similar UCNP/dye combinations for PDT in this manner have been explored with small animal models and demonstrated some success in tumour reduction and lifespan extension in Balb/c mouse models [115].

There have been limited studies as well with regard to using NIR excitation of UCNPs for uncaging reactions including the studies with regard to NO release described in the next section. In 2010 Carling *et al.* [118] prepared $NaYF_4$:Yb/Tm (30/0.5%) nanoparticles (45 nm) and loaded these by stirring with 3′,5′-(carboxymethoxy)benzoin acetate, which exchanged with the surface oleate ligands of these UCNPs. NIR excitation (980 nm, laser power 4.4 W, intensity of 550 W cm^{-2}) of an acetonitrile suspension of these decorated UCNPs led to cleavage (uncaging) of acetate from the organic chromophore. Note that 3′,5′-(carboxymethoxy)benzoin

chromophore absorbs only in the UV ($\lambda_{max} = 282$ nm), so it is light from the $^1D_2 \Rightarrow {}^3H_6$ emission of Tm^{3+} at 290 nm that is necessary to trigger this photoreaction, hence the relatively high laser intensity needed. In a more directly biological application Yang *et al.* [119] prepared $NaYF_4$:Yb/Tm(20/0.2%)@$NaYF_4$ core : shell UCNPs (approx. 50 nm) coated with a thiolated SiO_2 layer which was conjugated to D-luciferin caged with a 1-(2-nitrophenyl)ethyl group. The absorption band of the photocage overlaps with an upconverted UV emission band of Tm^{3+}($^1I_6 \Rightarrow {}^4F_3$, $^1D_2 \Rightarrow {}^3H_6$), so D-luciferin was released as the result of NIR excitation. These conjugated UCNPs were taken up by C6 glioma cells, and the D-luciferin was uncaged upon 980 nm irradiation for imaging of the firefly luciferase (fLuc) reporter gene, a commonly used bioluminescent probe. In addition, this conjugate and the fLuc enzyme were subcutaneously injected into living mice, and the bioluminescence was measured by using an *in vivo* imaging system. This proof of concept experiment demonstrates how the combination of UNCPs and NIR excitation might be used to deliver bioactive molecules to living systems.

(c) NO uncaging using upconversion nanoparticles

Studies in our laboratories [120] have now shown that assemblies based on $NaYF_4$:Yb/Er(20/2%)@$NaYF_4$ core : shell UCNPs can trigger the uncaging of NO from the iron/sulfur/nitrosyl cluster Roussin's black salt anion $Fe_4S_3(NO)_7^-$ (**RBS**, Na^+ salt). Photolysis of **RBS** at UV/visible wavelengths had previously been shown to release biologically relevant concentrations of NO in aerobic solutions [121,122]. Flash and continuous photolysis studies have also defined the stoichiometry (equation (5.1)) and mechanism of the photoreaction pathway in aqueous media [1,123]. Notably, aqueous **RBS** is stable in the dark and does not show any absorbance at 980 nm or any photochemistry when subjected to irradiation with a 980 nm CW laser.

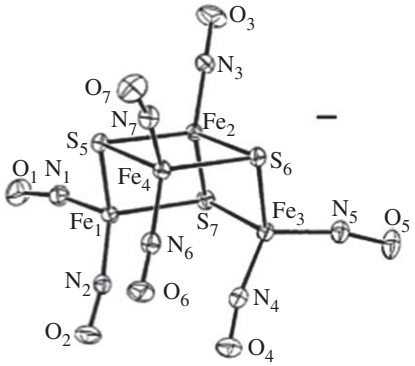

$$\xrightarrow[O_2]{h\nu} 3.9\ Fe^{2+} + 5.9\ NO + 3S^{2-} + \text{other products} \qquad (5.1)$$

The **RBS** anion was chosen as the caged form of NO for this proof-of-concept experiment owing to its strong visible absorption that overlays the visible emission bands of the β-$NaYF_4$:Yb/Er (20/2%)@$NaYF_4$ core:shell UCNPs used, especially the green ($^2H_{11/2} - {}^4I_{15/2}$, $^4S_{3/2} - {}^4I_{15/2}$) transitions (figure 8). Two kinds of **RBS**/UCNP combinations were prepared [120]. The first involved preparing core:shell UCNPs (average diameter 20 nm) then adding a silica layer approximately 10 nm thick. The silica coating not only makes these particles hydrophilic, but it can be treated with (3-aminopropyl)triethoxysilane to modify the surface with primary amines ($-NH_2$), which can be treated with acid to give cationic $-NH_3^+$ groups to attract the **RBS** anions. Irradiation of a stirred suspension of these UCNPs in a 42 μM solution of Na **RBS** with a 980 nm diode laser operating at approximately 1 W continuous output (intensity 5–30 W cm^{-2}) resulted in the generation of NO as detected by a GE Nitric Oxide Analyzer. NO output was linear with the irradiation time for a particular laser setting but showed nonlinear response to systematic increases in laser power from 1 to 4.5 W. A log/log plot gave a slope of 1.44 consistent with the power response of the emission at 550 nm (figure 7). Such nonlinear behaviour is very promising, since uncaging will be greatest at the focal point of the exciting light thus conveying an element of three-dimensional resolution to potential therapeutic applications.

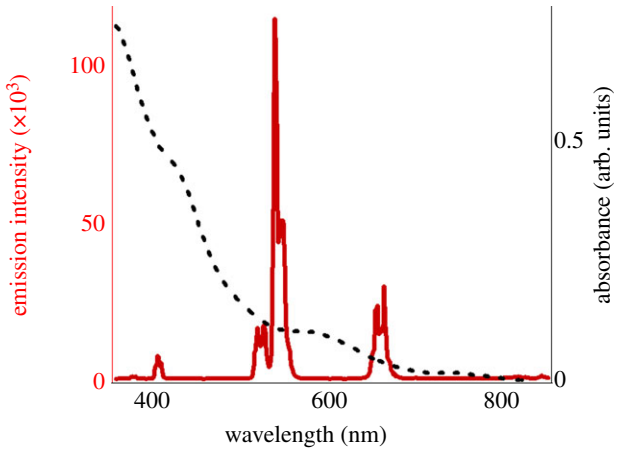

Figure 8. An overlay of the emission spectrum of an aqueous suspension of β-$NaYF_4$:Yb/Er (20/2%)@$NaYF_4$ core:shell UCNPs excited at 980 nm and the absorption spectrum of Na **RBS** (42 μM) in aqueous solution (dashed line) (J. V. Garcia 2012, unpublished data). (Online version in colour.)

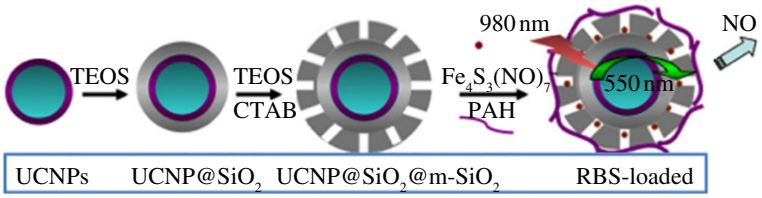

Scheme 4. Preparation of UCNPs with a mesoporous silica shell impregnated with Roussin's black salt (red dots), a photoactive NO generator, and coated with poly(allylamine hydrochloride). NIR irradiation leads to upconversion to wavelengths overlapping the **RBS** absorbance and NO uncaging. (Online version in colour.)

The second approach is illustrated in scheme 4. A mesoporous silica layer was added to the β-$NaYF_4$:Yb/Er (20/2%)@$NaYF_4$@SiO_2 core:shell:shell UCNPs to give nanomaterials with a total pore volume of 0.36 $cm^3\,g^{-1}$. These were then impregnated with Na **RBS** after which they were coated with poly(allylamine hydrochloride) to encapsulate the **RBS** into the unit. The **RBS** remained encapsulated after washing and isolating these nanoparticles but released NO upon irradiation with 980 nm light [120]. This is a particularly promising result since it suggests that these nanocarriers of the caged NO should remain intact during potential therapeutic upconversion applications.

For the first of the above proof of concept experiments, the overall efficiency is low, approximately 3×10^{-5} per cent, based on the estimated flux of NIR photons and the NO released. This is the product of several factors: the fraction of light absorbed by the nanocrystals, the quantum efficiency of upconversion, the fraction of upconverted light absorbed by the NO precursor, and the Φ_{NO} of NO uncaging from the precursor at that wavelength. In the present case, the low efficiency can be largely attributed to the low Φ_{NO} (approx. 0.001) for **RBS** under visible light excitation and the low upconversion efficiency (est. approx. 0.3%) [101]. However, these issues can be addressed by using photochemical precursors with more efficient quantum yields and perhaps by changing the compositions of the UCNPs, given that there have been reports of materials with greater upconversion efficiencies [102]. Thus, one can anticipate that the photonic efficiencies observed in these preliminary results can be improved very significantly, especially in the context that nanocarriers of the type described above offer the opportunity for very targeted uncaging of NO at therapeutically relevant sites.

6. Overview and summary

In this article, we have discussed potential applications of multi-photon excitation directed towards the photochemical uncaging of bioactive small molecules with particular emphasis on the promiscuous bioregulator NO. This approach offers the opportunity to use NIR light to access higher energy ESs that would otherwise require visible or ultraviolet light with SPE. Besides being less damaging, NIR wavelengths will penetrate much deeper into mammalian tissue, thus, in principle, would be less invasive to use in phototherapy. As in any phototherapy, the absorption of light, even in the NIR, will lead to some localized heating, which of course can have physiological consequences. For example, owing to a weak absorption band by water at approximately 980 nm [112], it may be desirable to design multi-photon absorbers and UCNPs that function at somewhat shorter NIR wavelengths to avoid this band, thus leading to more diffuse heat generation. Alternatively, the issue may be alleviated by using a pulsed light source and/or by increasing the concentration and efficiency of the photochemical precursor.

The other advantage of multi-photon excitation is the nonlinear response of the induced photochemistry to the excitation intensity. The expected photochemistry would occur primarily at the focal point of the excitation beam, and therefore would provide three-dimensional resolution. With regard to NO delivery, we have primarily discussed the use of dyes and QDs with high two-photon absorption cross sections for simultaneous TPE and of lanthanoid ion-doped UCNPs as sensitizers for sequential absorption of NIR photons to facilitate the uncaging process. The UCNPs offer a key advantage relative to simultaneous TPE, namely that the excitation intensities required are greatly reduced. Typically emission from UCNPs can be generated from continuous NIR diode lasers operating at $1–10^2\ \mathrm{W\,cm^{-2}}$, while the sources used for simultaneous TPE are typically ultrafast lasers with peak pulse intensities of $10^6–10^9\ \mathrm{W\,cm^{-2}}$. The former may be less damaging, although this is not certain, since the total energy delivered over a period of time would be comparable. The relative expense and ease of operation and maintenance of CW lasers are likely to prove much more important factors. Both approaches offer some promise for therapeutic NO uncaging, although it is clear that the possibilities have been barely explored and that moving such methods from the laboratory benchtop to therapy constitutes an enormous challenge.

Photochemical studies in the UCSB laboratory have long been supported by the Division of Chemistry of the US National Science Foundation (current grant CHE-1058794). Studies in the Fudan laboratory of F.Z. are supported by the National Science Foundation of China (NSFC grant 21101029). J.V.G. acknowledges a fellowship from the UCSB Partnership for International Research and Education in Electron Chemistry and Catalysis at Interfaces funded by the US National Science Foundation (NSF-OISE-0968399).

References

1. Bourassa JL, DeGraff W, Kudo S, Wink DA, Mitchell JB, Ford PC. 1997 Photochemistry of Roussin's red salt, $Na_2[Fe_2S_2(NO)_4]$, and of Roussin's black salt, $NH_4[Fe_4S_3(NO)_7]$. *In situ* nitric oxide generation to sensitize γ-radiation induced cell death. *J. Am. Chem. Soc.* **119**, 2853–2861. (doi:10.1021/JA963914N)
2. Ford PC. 2008 Polychromophoric metal complexes for generating the bioregulatory agent nitric oxide by single- and two-photon excitation. *Acc. Chem. Res.* **41**, 190–200. (doi:10.1021/ar700128y)
3. Ostrowski AD, Ford PC. 2009 Metal complexes as photochemical nitric oxide precursors: potential applications in the treatment of tumors. *Dalton Trans.* **28**, 10 660–10 669. (doi:10.1039/b912898k)
4. Rimmer RD, Richter H, Ford PC. 2010 A photochemical precursor for carbon monoxide release in aerated aqueous media. *Inorg. Chem.* **49**, 1180–1185. (doi:10.1021/ic902147n)
5. Rimmer RD, Pierri AE, Ford PC. 2012 Photochemically activated carbon monoxide release for biological targets. Toward developing air-stable photoCORMs labilized by visible light. *Coord. Chem. Rev.* **256**, 1509–1519. (doi:10.1016/j.ccr.2011.12.009)
6. Ignarro LJ. 2010 *Nitric oxide: biology and pathobiology*, 2nd edn. Burlington, MA: Elsevier Inc.

7. Mitchell JB, Wink DA, DeGraff W, Gamson J, Keefer LK, Krishna MC. 1993 Hypoxic mammalian-cell radiosenistization by nitric oxide. *Cancer Res*. **53**, 5845–5848.
8. Garthwaite J. 2010 New insight into the functioning of nitric oxide-receptive guanylyl cyclase: physiological and pharmacological implications. *Mol. Cell. Biochem.* **334**, 221–232. (doi:10.1007/s11010-009-0318-8)
9. Mocellin S, Bronte V, Nitti D. 2007 Nitric oxide, a double edged sword in cancer biology: searching for therapeutic opportunities. *Med. Res. Rev.* **27**, 317–352. (doi:10.1002/med.20092)
10. Rose MJ, Fry NL, Marlow R, Hinck L, Mascharak PK. 2008 Sensitization of ruthenium nitrosyls to visible light via direct coordination of the dye resorufin: trackable NO donors for light-triggered NO delivery to cellular targets. *J. Am. Chem. Soc.* **130**, 8834–8846. (doi:10.1021/ja801823f)
11. Fukumura D, Kashiwagi S, Jain RK. 2006 The role of nitric oxide in tumour progression. *Nat. Rev. Cancer* **6**, 521–534. (doi:10.1038/nrc1910)
12. Hirst D, Robson T. 2010 Nitric oxide in cancer therapeutics: interaction with cytotoxic chemotherapy. *Curr. Pharmaceut. Des.* **16**, 411–420. (doi:10.2174/138161210790232185)
13. Olson SY, Garbana HJ. 2008 Regulation of apoptosis-related genes by nitric oxide in cancer. *Nitric Oxide* **19**, 170–176. (doi:10.1016/j.niox.2008.04.005)
14. Ridnour LA, Thomas DD, Switzer C, Flores-Santana W, Isenberg JS, Ambs S, Roberts DD, Wink DA. 2008 Molecular mechanisms for discrete nitric oxide levels in cancer. *Nitric Oxide* **19**, 73–76. (doi:10.1016/j.niox.2008.04.006)
15. Jöbsis FF. 1977 Noninvasive, infrared monitoring of cerebral and myocardial oxygen sufficiency and circulatory parameters. *Science* **198**, 1264–1267. (doi:10.2307/1745848)
16. König K. 2000 Multiphoton microscopy in life sciences. *J. Microsc.* **200**, 83–104. (doi:10.1046/j.1365-2818.2000.00738.x)
17. Smith AM, Mancini MC, Nie S. 2009 Second window for *in vivo* imaging. *Nat. Nanotechnol.* **4**, 710–711. (doi:10.1038/nnano.2009.326)
18. Conrado CL, Wecksler S, Egler C, Magde D, Ford PC. 2004 Synthesis and photochemical properties of a novel iron–sulfur–nitrosyl cluster derivatized with the pendant chromophore protoporphyrin IX. *Inorg. Chem.* **43**, 5543–5549. (doi:10.1021/ic049459a)
19. Novais da Rocha Z, Galvao de Lima R, Doro FG, Tfouni E, Santana da Silva R. 2008 Photochemical production of nitric oxide from a nitrosyl phthalocyanine ruthenium complex by irradiation with light in the phototherapeutic window. *Inorg. Chem. Commun.* **11**, 737–740. (doi:10.1016/j.inoche.2008.03.019)
20. Rose MJ, Mascharak PK. 2008 Photoactive ruthenium nitrosyls: effects of light and potential application as NO donors. *Coord. Chem. Rev.* **252**, 2093–2114. (doi:10.1016/j.ccr.2007.11.011)
21. Hoffman-Luca CG, Eroy-Reveles AA, Alvarenga J, Mascharak PK. 2009 Syntheses, structures, and photochemistry of manganese nitrosyls derived from designed Schiff base ligands: potential NO donors that can be activated by near-infrared light. *Inorg. Chem.* **48**, 9104–9111. (doi:10.1021/ic900604j)
22. Ostrowski AD *et al.* 2011 Photochemistry of *trans*-Cr(cyclam)(ONO)2^{+}, a nitric oxide precursor. *Inorg. Chem.* **50**, 4453–4462. (doi:10.1021/ic200094x).
23. Wagenknecht PS, Ford PC. 2011 Metal centered ligand field excited states: their roles in the design and performance of transition metal based photochemical molecular devices. *Coord. Chem. Rev.* **255**, 591–616. (doi:10.1016/j.ccr.2010.11.016)
24. DeRosa F, Bu X, Ford PC. 2005 New chromium(III) complexes for photochemical nitric oxide generation from coordinated nitrite. The synthesis and photochemistry of macrocyclic complexes with pendant chromophores, *trans*-$[Cr(L)(ONO)_2]BF_4$. *Inorg. Chem.* **44**, 4157–4165. (doi:10.1021/ic048311o)
25. Neuman D, Ostrowski AD, Mikhailovsky AA, Absalonson RO, Ford PC. 2008 Quantum dot fluorescence quenching pathways of electrostatic assemblies with Cr(III) complexes. Sensitized nitric oxide production from *trans*-Cr(cyclam)$(ONO)_2^+$. *J. Am. Chem. Soc.* **130**, 168–175. (doi:10.1021/ja074164s)
26. He GS, Tan L-S, Zheng Q, Prasad PN. 2008 Multiphoton absorbing materials: molecular designs, characterizations, and applications. *Chem. Rev.* **108**, 1245–1330. (doi:10.1021/cr050054x)
27. Pedersen BW, Breitenbach T, Redmond RW, Ogilby PR. 2010 Two-photon irradiation of an intracellular singlet oxygen photosensitizer: achieving localized sub-cellular excitation in spatially-resolved experiments. *Free Rad. Res.* **44**, 1383–1397. (doi:10.3109/10715762.2010.515221)

28. Denk W, Strickler JH, Webb WW. 1990 Two-photon laser scanning fluorescence microscopy. *Science* **248**, 73–76. (doi:10.1126/science.2321027)
29. So PTC, Dong CY, Masters BR, Berland KM. 2000 Two-photon excitation fluorescence microscopy. *Annu. Rev. Biomed. Eng.* **2**, 399–429. (doi:10.1146/annurev.bioeng.2.1.399)
30. Oar MA *et al.* 2006 Light-harvesting chromophores with metalated porphyrin cores for tuned photosensitization of singlet oxygen via two-photon excited FRET. *Chem. Mater.* **18**, 3682–3692. (doi:10.1021/cm0606070).
31. Rumi M, Barlow S, Wang J, Perry JW, Marder SR. 2008 Two-photon absorbing materials and two-photon-induced chemistry. *Adv. Polym. Sci.* **213**, 1–95. (doi:10.1007/978-3-540-69450-2)
32. Pawlicki M, Collins HA, Denning RG, Anderson HL. 2009 Two-photon absorption and the design of two-photon dyes. *Angew. Chem. Int. Ed.* **48**, 3244–3266. (doi:10.1002/anie.200805257)
33. Dayal S, Burda C. 2008 Semiconductor quantum dots as two-photon sensitizers. *J. Am. Chem. Soc.* **130**, 2890–2891. (doi:10.1021/ja0781285)
34. Fowley C, Nomikou N, McHale AP, McCarron PA, McCaughan B, Callan JF. 2012 Water soluble quantum dots as hydrophilic carriers and two-photon excited energy donors in photodynamic therapy. *J. Mater. Chem.* **22**, 6456–6462. (doi:10.1039/c2jm00096b)
35. Liu Y, Chen P, Wang ZH, Bian F, Lin L, Chang SJ, Mu GG. 2009 Efficient two-photon absorption of CdSe–CdS/ZnS core-multishell quantum dots under the excitation of near-infrared femtosecond pulsed laser. *Laser Phys.* **19**, 1886–1890. (doi:10.1134/S1054660X09170113)
36. Pu SC, Yang MJ, Hsu CC, Lai CW, Hsieh CC, Lin SH, Cheng YM, Chou PT. 2006 The empirical correlation between size and two-photon absorption cross section of CdSe and CdTe quantum dots. *Small* **2**, 1308–1313. (doi:10.1002/smll.200600157)
37. Ustione A, Piston DW. 2011 A simple introduction to multiphoton microscopy. *J. Microsc.* **243**, 221–226. (doi:10.1111/j.1365-2818.2011.03532.x)
38. Pass H. 1993 Photodynamic therapy in oncology: mechanisms and clinical use. *J. Natl Cancer Inst.* **85**, 443–456. (doi:10.1093/jnci/85.6.443)
39. MacDonald IJ, Dougherty TJ. 2001 Basic principles of photodynamic therapy. *J. Porphyrins Phthalocyanins* **5**, 105–129. (doi:10.1002/jpp.328)
40. Phillips D. 2011 Toward targeted photodynamic therapy. *Pure Appl. Chem.* **83**, 733–748. (doi:10.1351/PAC-CON-11-01-05)
41. Kim S, Ohulchanskyy TY, Pudavar HE, Pandey RK, Prasad PN. 2007 Organically modified silica nanoparticles co-encapsulating photosensitizing drug and aggregation-enhanced two-photon absorbing fluorescent dye aggregates for two-photon photodynamic therapy. *J. Am. Chem. Soc.* **129**, 2669–2675. (doi:10.1021/ja0680257)
42. Collins HA *et al.* 2008 Blood-vessel closure using photosensitizers engineered for two-photon excitation. *Nat. Photon.* **2**, 420–424. (doi:10.1038/nphoton.2008.100)
43. Pettit DL, Wang SSH, Gee KR, Augustine GJ. 1997 Chemical two-photon uncaging: a novel approach to mapping glutamate receptors. *Neuron* **19**, 465–471. (doi:10.1016/S0896-6273(00)80361-X)
44. Furuta T, Wang SSH, Dantzker JL, Dore TM, Bybee WJ, Callaway EM, Denk W, Tsien RY. 1999 Brominated 7-hydroxycoumarin-4-ylmethyls: photolabile protecting groups with biologically useful cross-sections for two photon photolysis. *Proc. Natl Acad. Sci. USA* **96**, 1193–1200. (doi:10.1073/pnas.96.4.1193)
45. Warther D, Gug S, Specht A, Bolze F, Nicoud JF, Mourot A, Goeldner M. 2010 Two-photon uncaging: new prospects in neuroscience and cellular biology. *Biorg. Med. Chem.* **18**, 7753–7758. (doi:10.1016/j.bmc.2010.04.084)
46. Salierno M, Marceca E, Peterka DS, Yuste R, Etchenique R. 2010 A fast ruthenium polypyridine cage complex photoreleases glutamate with visible or IR light in one and two photon regimes. *J. Inorg. Biochem.* **104**, 418–422. (doi:10.1016/j.jinorgbio.2009.12.004)
47. Kantevari S, Matsuzaki M, Kanemoto Y, Kasai H, Ellis-Davies GCR. 2010 Two-color, two-photon uncaging of glutamate and GABA. *Nat. Meth.* **7**, 123–125. (doi:10.1038/NMETH.1413)
48. Matsuzaki M, Hayama T, Kasai H, Ellis-Davies GCR. 2010 Two-photon uncaging of γ-aminobutyric acid in intact brain tissue. *Nat. Chem. Biol.* **6**, 255–257. (doi:10.1038/NCHEMBIO.321)
49. Noguchi J, Nagaoka A, Watanabe S, Ellis-Davies GCR, Kitamura K, Kano M, Matsuzaki M, Kasai H. 2011 *In vivo* two-photon uncaging of glutamate revealing the structure–function

relationships of dendritic spines in the neocortex of adult mice. *J. Physiol.* **589**, 2447–2457. (doi:10.1113/jphysiol.2011.207100)
50. Donato L *et al.* 2012 Water-soluble, donor–acceptor biphenyl derivatives in the 2-(*o*-nitrophenyl)propyl series: highly efficient two-photon uncaging of the neurotransmitter aminobutyric acid at 800 nm. *Angew. Chem. Int. Ed.* **51**, 1840–1843. (doi:10.1002/anie.201106559)
51. Nikolenko V, Yuste R, Zayat L, Baraldo LM, Etchenique R. 2005 Two-photon uncaging of neurochemicals using inorganic metal complexes. *Chem. Commun.* 1752–1754. (doi:10.1039/b418572b)
52. Lin QN, Huang Q, Li CY, Bao CY, Liu ZZ, Li FY, Zhu LY. 2010 Anticancer drug release from a mesoporous silica based nanophotocage regulated by either a one- or two-photon process. *J. Am. Chem. Soc.* **132**, 10 645–10 647. (doi:10.1021/ja103415t)
53. Sun L, Yang Y, Dong CM, Wei Y. 2011 Two-photon-sensitive and sugar-targeted nanocarriers from degradable and dendritic amphiphiles. *Small* **7**, 401–406. (doi:10.1002/smll.201001729)
54. Kumar S, Allard JF, Morris D, Dory YL, Lepage M, Zhao Y. 2012 Near-infrared light sensitive polypeptide block copolymer micelles for drug delivery. *J. Mater. Chem.* **22**, 7252–7257. (doi:10.1039/c2jm16380b)
55. Kim HC, Hartner S, Hampp N. 2008 Single- and two-photon absorption induced photocleavage of dimeric coumarin linkers: therapeutic versus passive photocleavage in ophthalmologic applications. *J. Photochem. Photobiol. A* **197**, 239–244. (doi:10.1016/j.jphotochem.2007.12.032)
56. Conrado CL, Bourassa JL, Egler C, Wecksler S, Ford PC. 2003 Photochemical investigation of Roussin's red salt esters: $Fe_2(\mu\text{-}SR)_2(NO)_4$. *Inorg. Chem.* **42**, 2288–2293. (doi:10.1021/ic020309e)
57. Baker ES, Bushnell JE, Wecksler SR, Lim MD, Manard ME, Dupuis NF, Ford PC, Bowers MT. 2005 Probing shapes of bichromophoric metal-organic complexes using ion mobility mass spectrometry. *J. Am. Chem. Soc.* **127**, 18 222–18 228. (doi:10.1021/ja0553699)
58. Wecksler S, Mikhailovsky A, Ford PC. 2004 Photochemical production of nitric oxide via two photon excitation with NIR light. *J. Am. Chem. Soc.* **126**, 13 566–13 567. (doi:10.1021/ja045710+)
59. Goyan RL, Cramb DT. 2000 Near-infrared two-photon excitation of protoporphyrin IX: photodynamics and photoproduct generation. *Photochem. Photobiol.* **72**, 821–827. (doi:10.1562/0031-8655(2000)0720821NITPEO2.0.CO2)
60. Wecksler SR, Mikhailovsky A, Korystov D, Ford PC. 2006 A two-photon antenna for photochemical delivery of nitric oxide from a water-soluble, dye-derivatized iron nitrosyl complex using NIR light. *J. Am. Chem. Soc.* **126**, 3831–3837. (doi:10.1021/ja057977u)
61. Wecksler SR, Mikhailovsky A, Korystov D, Buller F, Kannan R, Tan L-S, Ford PC. 2007 Single- and two-photon properties of a dye-derivatized Roussin's red salt ester ($Fe_2(\mu\text{-}RS)_2(NO)_4$)) with a large TPA cross section. *Inorg. Chem.* **46**, 395–402. (doi:10.1021/ic0607336)
62. Xu C, Webb WW. 1996 Measurement of two-photon excitation cross sections of molecular fluorophores with data from 690 to 1050 nm. *J. Opt. Soc. Am. B* **13**, 481–491. (doi:10.1364/JOSAB.13.000481)
63. Zheng Q, Bonoiu A, Ohulchanskyy TY, He GS, Prasad PN. 2008 Water-soluble two-photon absorbing nitrosyl complex for light-activated therapy through nitric oxide release. *Mol. Pharm.* **5**, 389–398. (doi:10.1021/mp700117s)
64. Tsuchiya K, Yoshizumi M, Houchi H, Mason RP. 2000 Nitric oxide-forming reaction between the iron-*N*-methyl-D-glucamine dithiocarbamate complex and nitrite. *J. Biol. Chem.* **275**, 1551–1556. (doi:10.1074/jbc.275.3.1551)
65. Hishikawa K, Nakagawa H, Furuta T, Fukuhara K, Tsumoto H, Suzuki T, Miyata N. 2009 Photoinduced nitric oxide release from a hindered nitrobenzene derivative by two-photon excitation. *J. Am. Chem. Soc.* **131**, 7488–7489. (doi:10.1021/ja8093668)
66. Hishikawa K, Nakagawa H, Furuta T, Fukuhara K, Tsumoto H, Suzuki T, Miyata N. 2010 Multiple bond-conjugated photoinduced nitric oxide releaser working with two-photon excitation. *Bioorg. Med. Chem. Lett.* **20**, 302–305. (doi:10.1016/j.bmcl.2009.10.120)
67. Eliseeva SV, Bunzli J-CG. 2010 Lanthanide luminescence for functional materials and bio-sciences. *Chem. Soc. Rev.* **39**, 189–227. (doi:10.1039/B905604C)
68. Sivakumar S, Diamente PR, van Veggel FCJM. 2006 Silica-coated Ln^{3+}-doped LaF_3 nanoparticles as robust down- and upconverting biolabels. *Chem. Eur. J.* **12**, 5878–5884. (doi:10.1002/chem.200600224)

69. Wang F, Liu X. 2009 Recent advances in the chemistry of lanthanide-doped upconversion nanocrystals. *Chem. Soc. Rev.* **38**, 976–989. (doi:10.1039/b809132n)
70. Vennerberg D, Lin Z. 2011 Upconversion nanocrystals: synthesis, properties, assembly and applications. *Sci. Adv. Mater.* **3**, 26–40. (doi:10.1166/sam.2011.1137)
71. Chatterjee DK, Gnanasammandhan MK, Zhang Y. 2010 Small upconverting fluorescent nanoparticles for biomedical applications. *Small* **6**, 2781–2795. (doi:10.1002/smll.201000418)
72. Haase M, Schäfer H. 2011 Upconverting nanoparticles. *Angew. Chem. Int. Ed.* **50**, 5808–5829. (doi:10.1002/anie.201005159)
73. Ovsyakin VV, Feofilov PP. 1966 Cooperative sensitization of luminescence in crystal activated with rare earth ions. *Sov. Phys. JETP Lett.* **4**, 317–318.
74. Xie P, Rand SC. 1992 Visible cooperative upconversion laser in Er:$LiYF_4$. *Opt. Lett.* **17**, 1198–1200. (doi:10.1364/OL.17.001198)
75. Weber M (ed.) 1998 *Selected papers on photoluminescence of inorganic solids*. SPIE Milestone Series MS150. Bellingham, WA: SPIE Press.
76. Hwang B-C, Jiang S, Luo T, Watson J, Sorbello G, Peyghambarian N. 2000 Cooperative upconversion and energy transfer of new high Er^{3+}- and $Yb^{3+} - Er^{3+}$ -doped phosphate glasses. *J. Opt. Soc. Am. B* **17**, 833–839. (doi:10.1364/JOSAB.17.000833)
77. Sivakumar S, van Veggel FCJM. 2007 Red, green, and blue light through cooperative upconversion in sol-gel thin films made with $Yb_{0.80}La_{0.15}Tb_{0.05}F_3$ and $Yb_{0.80}La_{0.15}Eu_{0.05}F_3$ nanoparticles. *J. Display Technol.* **3**, 176–183. (doi:10.1109/JDT.2007.896749)
78. Auzel F. 2004 Upconversion and anti-Stokes processes with f and d ions in solids. *Chem. Rev.* **104**, 139–173. (doi:10.1021/cr020357g)
79. Zhang F *et al.* 2007 Uniform nanostructured arrays of sodium rare-earth fluorides for highly efficient multicolor upconversion luminescence. *Angew. Chem. Int. Ed.* **46**, 7976–7979. (doi:10.1002/anie.200702519)
80. Wong H-T, Chan HLW, Hao J. 2010 Towards pure near-infrared to near-infrared upconversion of multifunctional GdF_3:Yb^{3+}, Tm^{3+} nanoparticles. *Opt. Exp.* **18**, 6123–6130. (doi:10.1364/OE.18.006123)
81. Menyuk N, Dwight K, Pierce JW. 1972 $NaYF_4$: Yb,Er—an efficient upconversion phosphor. *Appl. Phys. Lett.* **21**, 159–161. (doi:10.1063/1.1654325)
82. Wang X, Zhuang J, Peng Q, Li Y. 2005 A general strategy for nanocrystal synthesis. *Nature* **437**, 121–124. (doi:10.1038/nature03968)
83. Wang F, Chatterjee DK, Li ZQ, Zhang Y, Fan XP, Wang MQ. 2006 Synthesis of polyethylenimine/$NaYF_4$ nanoparticles with upconversion fluorescence. *Nanotechnology* **17**, 5786–5791. (doi:10.1088/0957-4484/17/23/013)
84. Zhang T, Guo H, Qiao YM. 2009 Facile synthesis, structural and optical characterization of LnF_3:RE nanocrystals by ionic liquid-based hydrothermal process. *J. Luminesc.* **129**, 861–866. (doi:10.1016/j.jlumin.2009.03.011)
85. Naczynski DJ, Andelman T, Pal D, Chen S, Riman RE, Roth CM, Moghe PV. 2010 Albumin nanoshell encapsulation of near-infrared-excitable rare-earth nanoparticles enhances biocompatibility and enables targeted cell imaging. *Small* **6**, 1631–1640. (doi:10.1002/smll.200902403)
86. Yi GS, Chow GM. 2006 Synthesis of hexagonal-phase $NaYF_4$:Yb,Er and $NaYF_4$:Yb,Tm nanocrystals with efficient up-conversion fluorescence. *Adv. Funct. Mater.* **16**, 2324–2329. (doi:10.1002/adfm.200600053)
87. Boyer F *et al.* 2010 Simultaneous phase and size control of upconversion nanocrystals through lanthanide doping. *Nature* **463**, 1061–1065. (doi:10.1038/nature08777)
88. Ostrowski AD, Chan EM, Gargas DJ, Katz EM, Han G, Schuck PJ, Milliron DJ, Cohen BE. 2012 Controlled synthesis and single-particle imaging of bright, sub-10 nm lanthanide-doped upconverting nanocrystals. *ACS Nano* **6**, 2686–2692. (doi:10.1021/nn3000737)
89. Yi G-S, Chow G-M. 2007 Water-soluble $NaYF_4$:Yb,Er(Tm)/$NaYF_4$/polymer core/shell/shell nanoparticles with significant enhancement of upconversion fluorescence. *Chem. Mater.* **19**, 341–343. (doi:10.1021/cm062447y)
90. Wang F, Wang J, Liu X. 2010 Direct evidence of a surface quenching effect on size-dependent luminescence of upconversion nanoparticles. *Angew. Chem. Int. Ed.* **49**, 7456–7460. (doi:10.1002/anie.201003959)
91. Stöber W, Fink A, Bohn E. 1968 Controlled growth of monodisperse silica spheres in the micron size range. *J. Colloid Interface Sci.* **26**, 62–69. (doi:10.1016/0021-9797(68)90272-5)

92. Beck JS *et al.* 1992 A new family of mesoporous molecular sieves prepared with liquid crystal templates. *J. Am. Chem. Soc.* **114**, 10 835–10 843. (doi:10.1021/ja00053a020)
93. Chenite A, Le Page Y, Sayari A. 1995 Direct TEM imaging of tubules in calcined MCM-41 type mesoporous materials. *Chem. Mater.* **7**, 1015–1019. (doi:10.1021/cm00053a031)
94. Holm BA, Bergey EJ, De T, Rodman DJ, Kapoor R, Levy L, Friend CS, Prasad PN. 2002 Nanotechnology in biomedical applications. *Mol. Cryst. Liq. Cryst.* **374**, 589–598. (doi:10.1080/713738279)
95. Nagata H, Takimura M, Yamasaki Y, Nakahira A. 2006 Syntheses and characterization of bulky mesoporous silica MCM-41 by hydrothermal hot-pressing method. *Mater. Trans.* **47**, 2103–2105. (doi:10.2320/matertrans.47.2103)
96. Qian HS, Guo HC, Ho PC-L, Mahendran R, Zhang Y. 2009 Mesoporous-silica-coated up-conversion fluorescent nanoparticles for photodynamic therapy. *Small* **5**, 2285–2290. (doi:10.1002/smll.200900692)
97. Canton G, Ricco R, Marinello F, Carmignato S, Enrichi F. 2011 Modified Stöber synthesis of highly luminescent dye-doped silica nanoparticles. *J. Nanopart. Res.* **13**, 4349–4356. (doi:10.1007/s11051-011-0382-3)
98. Xu H, Cheng L, Wang C, Ma X, Li Y, Liu Z. 2011 Polymer encapsulated upconversion nanoparticle/iron oxide nanocomposites for multimodal imaging and magnetic targeted drug delivery. *Biomaterials* **32**, 9364–9373. (doi:10.1016/j.biomaterials.2011.08.053)
99. Jiang S, Zhang Y, Lim KM, Sim EKW, Ye L. 2009 NIR-to-visible upconversion nanoparticles for fluorescent labeling and targeted delivery of siRNA. *Nanotechnology* **20**, 155101. (doi:10.1088/0957-4484/20/15/155101).
100. Suyver JF, Grimm J, Krämer KW, Güdel HU. 2005 Highly efficient near-infrared to visible up-conversion process in $NaYF_4$: Er^{3+}, Yb^{3+}. *J. Luminesc.* **114**, 53–59. (doi:10.1016/j.jlumin.2004.11.012)
101. Boyer J-C, van Veggel FCJM. 2010 Absolute quantum yield measurements of colloidal $NaYF_4$: Er^{3+}, Yb^{3+} upconverting nanoparticles. *Nanoscale* **2**, 1417–1419. (doi:10.1039/c0nr00253d)
102. Page RH, Schaffers KI, Waide PA, Tassano JB, Payne SA, Krupke WF, Bischel WK. 1998 Upconversion-pumped luminescence efficiency of rare-earth-doped hosts sensitized with trivalent ytterbium. *J. Opt. Soc. Am. B* **15**, 996–1008. (doi:10.1364/JOSAB.15.000996)
103. Chatterjee DK, Rufaihah AJ, Zhang Y. 2008 Upconversion fluorescence imaging of cells and small animals using lanthanide doped nanocrystals. *Biomaterials* **29**, 937–943. (doi:10.1016/j.biomaterials.2007.10.051)
104. Nyk M, Kumar R, Ohulchanskyy TY, Bergey EJ, Prasad PN. 2008 High contrast *in vitro* and *in vivo* photoluminescence bioimaging using near infrared to near infrared up-conversion in Tm^{3+} and Yb^{3+} doped fluoride nanophosphors. *Nano Lett.* **8**, 3834–3838. (doi:10.1021/nl802223f)
105. Wang M, Mi C-C, Wang W-X, Liu C-H, Wu Y-F, Xu Z-R, Mao C-B, Xu S-K. 2009 Immunolabeling and NIR-excited fluorescent imaging of HeLa cells by using $NaYF_4$:Yb,Er upconversion nanoparticles. *ACS Nano* **3**, 1580–1586. (doi:10.1021/nn900491j)
106. Cheng L, Yang K, Li Y-G, Chen J-H, Wang C, Shao M-W, Lee S-T, Liu Z. 2011 Facile preparation of multifunctional upconversion nanoprobes for multimodal imaging and dual-targeted photothermal therapy. *Angew. Chem. Int. Ed.* **50**, 7385–7390. (doi:10.1002/anie.201101447)
107. Zhang F, Haushalter RC, Haushalter RW, Shi Y, Zhang Y, Ding K, Zhao D, Stucky GD. 2011 Rare-earth upconverting nanobarcodes for multiplexed biological detection. *Small* **7**, 1972–1976. (doi:10.1002/smll.201100629)
108. Salthouse C, Hilderbrand S, Weissleder R, Mahmood U. 2008 Design and demonstration of a small-animal up-conversion imager. *Opt. Exp.* **16**, 21 731–21 737. (doi:10.1364/OE.16.021731)
109. Hilderbrand SA, Shao FW, Salthouse C, Mahmood U, Weissleder R. 2009 Upconverting luminescent nanomaterials: application to *in vivo* bioimaging. *Chem. Commun.* 4188–4190. (doi:10.1039/b905927j)
110. Xiong L, Chen Z, Tian Q, Cao T, Xu C, Li F. 2009 High contrast upconversion luminescence targeted imaging *in vivo* using peptide-labeled nanophosphors. *Anal. Chem.* **81**, 8687–8694. (doi:10.1021/ac901960d)
111. Xiong L, Yang T, Yang Y, Xu C, Li F. 2010 Long-term *in vivo* biodistribution imaging and toxicity of polyacrylic acid-coated upconversion nanophosphors. *Biomaterials* **31**, 7078–7085. (doi:10.1016/j.biomaterials.2010.05.065)

112. Zhou J, Liu Z, Li F. 2012 Upconversion nanophosphors for small-animal imaging. *Chem. Soc. Rev.* **41**, 1323–1349. (doi:10.1039/c1cs15187h)
113. Ungun B, Prud'homme RK, Budijono SJ, Shan JN, Lim SF, Ju YG, Austin R. 2009 Nanofabricated upconversion nanoparticles for photodynamic therapy. *Opt. Exp.* **17**, 80–86. (doi:10.1364/OE.17.000080)
114. Guo H, Qian H, Idris NM, Zhang Y. 2010 Singlet oxygen-induced apoptosis of cancer cells using upconversion fluorescent nanoparticles as a carrier of photosensitizer. *Nanomedicine* **6**, 486–495. (doi:10.1016/j.nano.2009.11.004)
115. Wang C, Tao H, Cheng L, Liu Z. 2011 Near-infrared light induced *in vivo* photodynamic therapy of cancer based on upconversion nanoparticles. *Biomaterials* **32**, 6145–6154. (doi:10.1016/j.biomaterials.2011.05.007)
116. Lim ME, Lee YL, Zhang Y, Chu JJH. 2012 Photodynamic inactivation of viruses using upconversion nanoparticles. *Biomaterials* **33**, 1912–1920. (doi:10.1016/j.biomaterials.2011.11.033)
117. Cui S, Chen H, Zhu H, Tian J, Chi X, Qian Z, Achilefu S, Gu Y. 2012 Amphiphilic chitosan modified upconversion nanoparticles for *in vivo* photodynamic therapy induced by near-infrared light. *J. Mater. Chem.* **22**, 4861–4873. (doi:10.1039/C2JM16112E)
118. Carling CJ, Nourmohammadian F, Boyer JC, Branda NR. 2010 Remote-control photorelease of caged compounds using near-infrared light and upconverting nanoparticles. *Angew. Chem. Int. Ed.* **49**, 3782–3785. (doi:10.1002/anie.201000611)
119. Yang Y *et al.* 2012 *In vitro* and *in vivo* uncaging and bioluminescence imaging by using photocaged upconversion nanoparticles. *Angew. Chem. Int. Ed.* **51**, 3125–3129. (doi:10.1002/anie.201107919)
120. Garcia JV, Yang J, Shen D, Yao C, Li X, Stucky GD, Zhao DY, Ford PC, Zhang F. 2012 Near-infrared triggered release of caged nitric oxide using upconverting nanostructured materials. *Small* **8**, 3800–3805. (doi:10.1002/smll.201201213)
121. Flitney FW, Megson IL, Flitney DE, Butler AR. 1992 Iron–sulfur cluster nitrosyls, a novel class of nitric oxide generator: mechanism of vasodilator action on rat isolated tail artery. *Br. J. Pharmacol.* **107**, 842–848.
122. Flitney FW, Megson IL, Thomson JLM, Kennovin GD, Butler AR. 1996 Vasodilator responses of rat isolated tail artery enhanced by oxygen-dependent, photochemical release of nitric oxide from iron–sulphur–nitrosyls. *Br. J. Pharmacol.* **117**, 1549–1557.
123. Bourassa JL, Lee B, Bernard S, Schoonover J, Ford PC. 1999 Flash photolysis studies of Roussin's black salt anion. *Inorg. Chem.* **38**, 2947–2952. (doi:10.1021/ic981282v)